Modeling and Simulation of Robotic Finger Powered by Nylon Artificial Muscles

Lokesh Saharan[1]
Department of Mechanical Engineering,
Humanoid, Biorobotics and Smart Systems (HBS) Laboratory,
The University of Texas at Dallas,
800 W Campbell Rd,
Richardson, TX 75080
e-mail: lokeshkumar.saharan@utdallas.edu

Lianjun Wu[2]
Department of Mechanical Engineering,
Humanoid, Biorobotics and Smart Systems (HBS) Laboratory,
The University of Texas at Dallas,
800 W Campbell Rd,
Richardson, TX 75080
e-mail: lxw132630@utdallas.edu

Yonas Tadesse
Department of Mechanical Engineering,
Humanoid, Biorobotics and Smart Systems (HBS) Laboratory,
The University of Texas at Dallas,
800 W Campbell Rd,
Richardson, TX 75080
e-mail: yonas.tadesse@utdallas.edu

A robotic finger actuated by novel artificial muscles known as twisted and coiled polymer (TCP) muscles has been proposed as an inexpensive, yet high-performance component of a robotic hand in recent years. In this paper, the Euler–Lagrangian method coupled with an electro-thermo-mechanical model-based transfer function was used for the analysis of finger joints in the hand. Experiments were performed at three power magnitudes provided to the TCP muscles, and the output angular displacements of the index finger subtended corresponding to the power levels were measured. The measured input and output parameters were used for system identification. To elucidate how the new artificial muscle influences the finger motion, two types of numerical simulations were performed: force input simulation (FIS) using measured force as an input and power input simulation (PIS) using measured electrical power as an input. Results were quantified statistically, and the simulated data were compared with the experimental results. Sensitivity analysis was also presented to understand the effect of the mechanical properties on the system. This model will help in understanding the effect of the TCP muscles and other similar smart actuators on the dynamics of the robotic finger. [DOI: 10.1115/1.4044740]

Keywords: robotic finger, artificial muscles, smart materials, modeling, simulation and experiments, actuators and transmissions, cable-driven mechanisms, grasping and fixturing, multi-body dynamics and exoskeletons

1 Introduction

Several robotic hands, prosthetic devices, and exoskeletons have been developed to achieve comparable dexterity or surpass the capability of a human hand. The progress, summary, and challenges of such devices are discussed in the literature [1]. To exploit the actuation capabilities of the recently invented twisted and coiled polymer (TCP) [2] muscles, we have developed a 3D printable, lightweight, and compact hand [3]. TCP muscles are thermal actuators, which respond to the change in the temperature. The TCP muscles in this work are made out of sewing thread (nylon 6,6 fiber coated with silver, typically a nanometer thick) by twisting, coiling, and heat treatment processes. Figure 1 shows the picture of the robotic hand actuated by TCP muscles housed in the forearm and grasping some objects.

TCP muscles are soft actuators that have numerous advantages over their counterparts such as SMAs [4,5] in terms of low hysteresis, lightweight, low cost, easy availability, and manufacturability. TCP muscles have been used in an orthotic device named iGrab utilizing biomimetic actuation capabilities of these actuators [6], which is currently in the advanced development stage to be used on patients with muscular disorders. Due to their imperative features, TCP muscles have been used in similar applications for robotic/humanoid hand [7,8] and developing sensors [9,10]. Fabrication process and properties of these actuators, such as isometric and isothermal properties of TCPs, have been described in our previous works [11–13] as well as by other research groups [14–16].

The modeling and position control of the TCP muscle were presented in Ref. [17–19], and system identification for the TCP muscle was described by Yip and Niemeyer [20]. The limitation with the model as given in Ref. [20] is the force range, which is below 1 N. In this paper, we investigated a wide force range of the three-ply TCP muscle under certain given powers. Another system identification-based model was presented by Jafarzadeh et al. [21] for 1-ply muscle for a force of 110–540 mN. Arakawa et al. [22] also presented a system identification-based model to predict the dynamics of the system. Another approach is phenomenological modeling, as shown in Ref. [23], which predicted the temperature and displacement at lower loading conditions (applied load). However, their model is not demonstrated at high load and applied power. Hence, given the complexity of the system, we considered the black box model using experimental data for the modeling of TCP in this paper.

For a better understanding of the angular motion of the TCP muscle-actuated robotic finger, dynamic modeling is essential. Hence, we used Lagrangian dynamics [24] for analytical modeling of the finger since it has been used widely for dynamic analysis of several systems. We have used the Euler–Lagrangian (E–L)-based modeling in one of our previous works [6], but that work presented a simple E–L model without considering the model for the muscle. The focus of this work is Euler–Lagrangian modeling coupled with system identification-based electro-thermo-mechanical model of TCP, which has not been discussed in the literature.

The dynamic modeling equations were derived and verified using MATLAB® for a three-link underactuated robotic finger, and a Simulink® model was developed using these equations for simulation. The physical parameters and inertial properties of the hand were obtained from SolidWorks® model of the hand. The material properties of the TCP muscles were obtained from Ref. [3]. The relatively small order terms or insignificant contributing factors were ignored. The Simulink® model was solved based on the power and force profiles of the TCP muscles obtained experimentally during pulsed actuations. *Pulsed actuation* is defined as the Joule heating of the muscle using a high-intensity electrical power pulse for a short duration. When a square wave power at a relatively long duration is used for actuation, it is named as *regular actuation*.

[1]Present address: Department of Mechanical Engineering, The Pennsylvania State University, Erie, PA 16563.
[2]Present address: Department of Manufacturing Engineering, Georgia Southern University, Statesboro, GA 30460.

Contributed by the Mechanisms and Robotics Committee of ASME for publication in the Journal of Mechanisms and Robotics. Manuscript received January 29, 2019; final manuscript received August 17, 2019; published online September 5, 2019. Assoc. Editor: Tuhin Das.

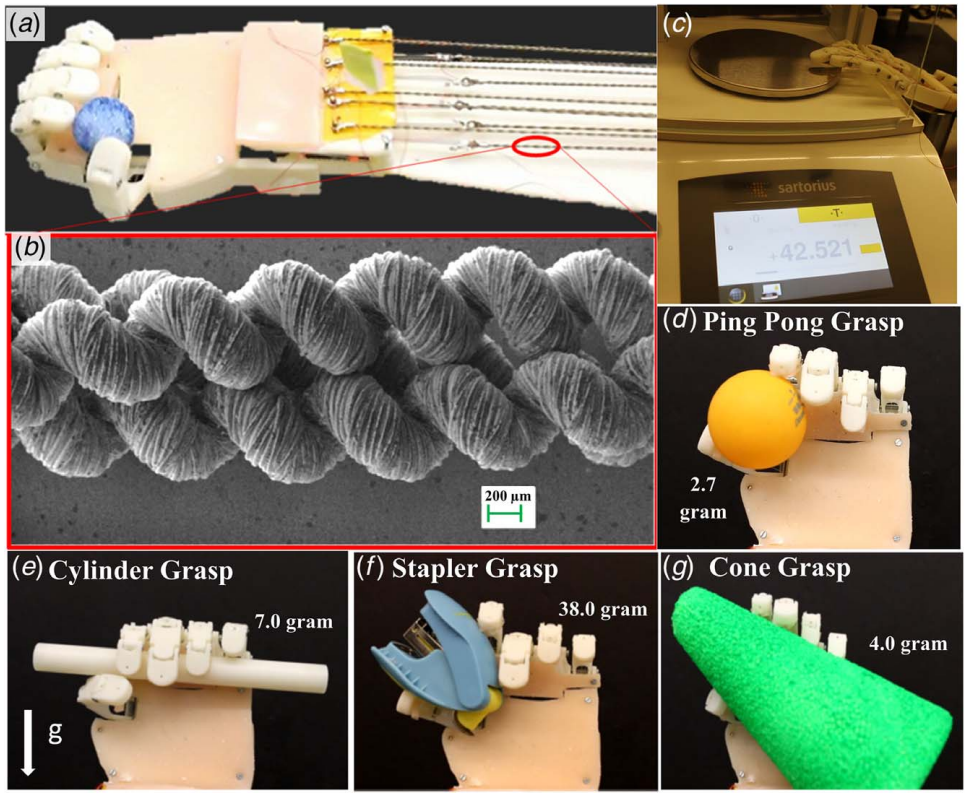

Fig. 1 A robotic hand actuated by TCP muscles: (*a*) overview of the hand, (*b*) microscopic image of a three-ply TCP muscle used in the hand, (c) the finger force against the surface of a scale, and (*d*)–(*g*) grasping various objects

The pulsed actuation is preferred for finger actuation since it provides a faster response/speed than the regular actuation.

The contributions of this paper are the following: (1) a detailed study on the coupling of the new TCP muscle and a robotic finger, (2) explicit equation sets that can be easily coded using the Simulink® model for studying the effect of parametric variation (sensitivity analysis), and (3) system identification of the coupled system (TCP muscle and robotic finger) and integration with the Euler–Lagrangian model, as well as experimental validation of joint angles with the simulation results.

2 Design of Robotic Hand Based on Twisted and Coiled Polymer Muscles

The fundamental design goal of many robotic or humanoid hands is to mimic the basic capabilities of the human hands, such as manipulating objects in space. Additional design goals are cost-effectiveness, lightweight, comfort, and responsiveness. It is challenging to replicate tactile sensation and dexterous manipulation at the same time in humanoid hands. However, the TCP hand meets some of the design goals of robotic hands—such as lightweight, low cost, and high actuation performance. Figure 2 shows the schematic diagram of the index finger (of TCP hand) and its force transmission system. It includes the arrangement of actuation system encompassing torsional springs, guide systems, tendons, and the TCP muscles housed in the forearm. In Fig. 2(*b*), the distal interphalangeal (DIP), proximal interphalangeal (PIP), and metacarpophalangeal (MCP) joints are shown, along with the grooves on the sides of each phalanx used to recess torsional springs. The torsional springs made of music wire were used in conjunction with the three-ply actuators to create finger extension/flexion.

We designed the hand for a humanoid robot equivalent to the size of a seven-year-old child [3,25]. All the solid models of the fingers

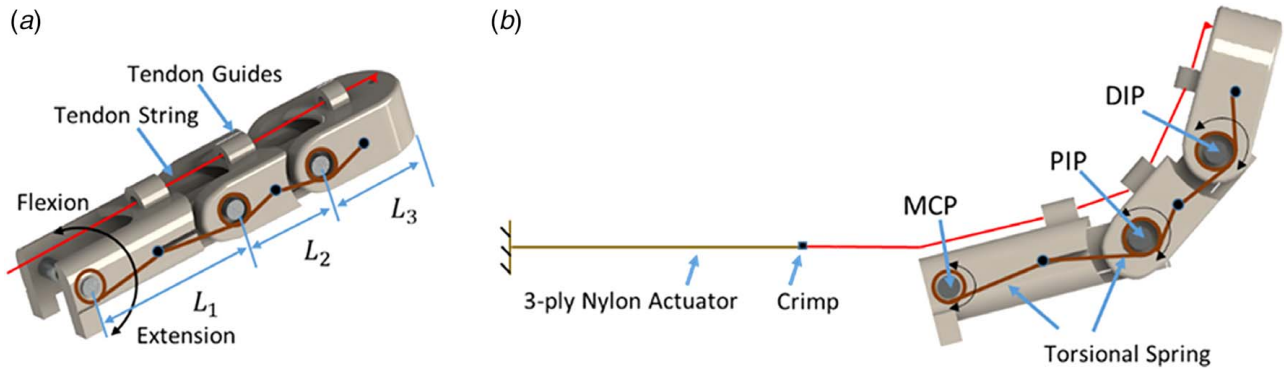

Fig. 2 CAD model of the index finger: (*a*) three-ply flexor muscles with torsional springs before actuation and (*b*) the hand during flexion

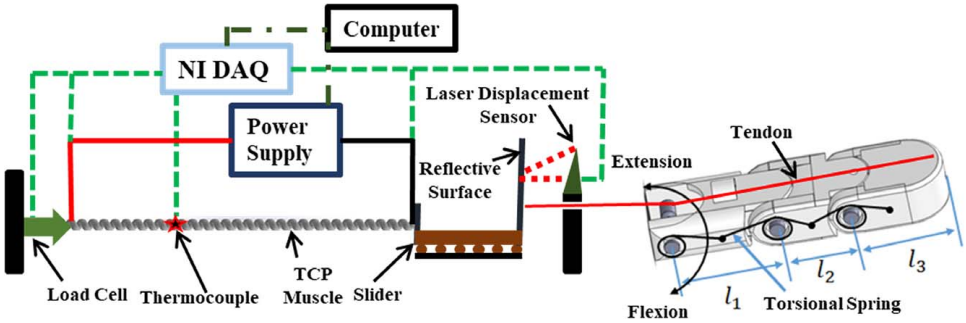

Fig. 3 Experimental setup for the measurement of the key parameters of the actuator (TCP muscle)

and hand parts were designed in SolidWorks®, and the parts were fabricated by a 3D printer using ABS plus (Stratasys®) material. The dimensions of the index finger were: $L_1 = 12$ mm, $L_2 = 9$ mm, and $L_3 = 12$ mm; The length of the muscle is 100 mm which was determined based on the required deformation that results in a maximum finger motion.

3 Experimental Characterization

3.1 Twisted and Coiled Polymer Muscles Actuation Study. Understanding the actuator force profile is essential to perform dynamic modeling of the entire system, and therefore, the experimental study was conducted on the three-ply TCP muscles. The experimental setup (Fig. 3) includes a load cell (Futek LSB200), laser displacement sensor (Keyence LK-G5000), a K-type thermocouple of 30 gauges (Omega®), a computer-controlled power supply (BK Precision® 9182), and a National Instrument DAQ.

We varied the magnitude of power (via varying current) supplied to the actuator and measured the force profile, and the results are shown in Fig. 4(*a*). The three different current values used for the pulsed actuation tests were 2.5 A, 2.7 A, and 2.9 A (1 s actuation time). TCP muscles appear slow at first glance because the results presented in this paper are under natural cooling. However, the actuators (and hence, the entire system) can operate at high frequency, up to 7 Hz [2]. For the current study, the measurement was done at a sampling rate of 1 kHz. It can be seen that the output force increases as the power increases. The effective force, approximately 2.5 N, was obtained at the initial prestress of 0.05 N. This force profile (Fig. 4(*b*)) was directly plugged into the Simulink® model for the simulation to predict the angular motion of the finger. In Section 3.2, we will discuss the system identification of the TCP muscle.

3.2 Twisted and Coiled Muscles Actuation Study System Identification. The TCP muscles are electrothermal transducers, which convert the electrical energy to thermal energy through

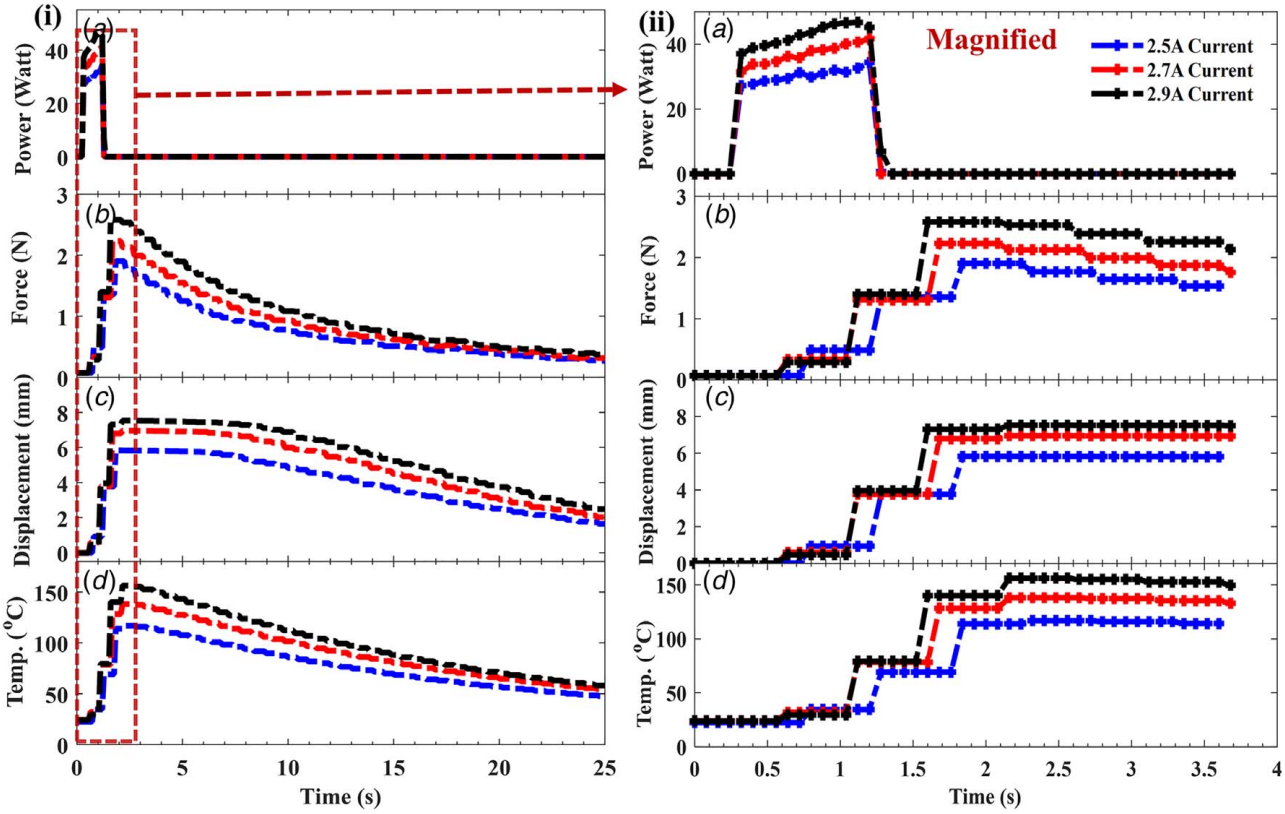

Fig. 4 Experimentally measured parameters of a three-ply muscle (100 mm in length) integrated in the hand and pulsed power: (*a*) power for three input current magnitudes, (*b*) force response during flexion of the finger, (c) linear tendon displacement, and (*d*) temperature produced in response to the input power

Table 1 Details of the transfer functions evaluated during the study

Temperature: Power		Force: Temperature	
Transfer function	Fitting (%)	Transfer function	Fitting (%)
$TF_{TP01} = \frac{4.017}{s + 0.05167}$	63	$TF_{FT01} = \frac{0.0002877}{s + 0.09062}$	37
$TF_{TP1} = \frac{-1.608\,s + 2.55}{s + 0.0542}$	72	$TF_{FT1} = \frac{0.02032\,s + 0.003318}{s + 0.2947}$	93
$TF_{TP02} = \frac{7.354}{s^2 + 1.688\,s + 0.1009}$	89	$TF_{FT02} = \frac{0.00172}{s^2 + 0.9002\,s + 0.2407}$	76
$TF_{TP002} = \frac{-2.072\,s + 6.622}{s^2 + 2.112\,s + 0.1259}$	90	$TF_{FT002} = \frac{0.02926\,s + 0.001831}{s^2 + 10.98\,s + 0.6438}$	48
$TF_{TP2} = \frac{0.01461\,s^2 - 2.036\,s + 6.712}{s^2 + 2.117\,s + 0.1263}$	90	$TF_{FT2} = \frac{0.01899\,s^2 + 0.002551\,s - 0.0001572}{s^2 + 0.3987\,s + 1.513e-06}$	96
$TF_{TP03} = \frac{44.64}{s^3 + 6.545\,s^2 + 11.02\,s + 0.6484}$	91	$TF_{FT03} = \frac{-4.8333e-05}{s^3 + 0.1595\,s^2 + 0.09401\,s + 1.626e-14}$	47
$TF_{TP3} = \frac{47.35\,s - 69.64}{s^3 + 57.31\,s^2 + 128.8\,s + 7.693}$	47	$TF_{FT3} = \frac{0.7941\,s - 0.1235}{s^3 + 0.27\,s^2 + 41.62\,s + 11.24}$	84

Joule heating, and then, the energy is converted to mechanical energy via lifting a load. The experimental data shown in Fig. 4 were used for the system identification to study the relationship between the power (P), the force (F), and temperature (T). The transfer function models were estimated in the system identification application in MATLAB® specifying the initial condition via instrument variable approach (VI) and keeping the default values for the rest of the parameters.

The physical model of the TCP muscle (temperature: power) is a first-order system, under certain conditions such as constant convective heat transfer coefficient as showed by Arakawa et al. [22], but we used a higher-order system for the coupled system (TCP and finger joint with torsional springs) and found a good fitting (Table 1, left). To understand the actuations, we started with a lumped capacitance model of thermal actuators:

$$mc_p \frac{dT}{dt} = P - hA_c(T - T_\infty) \tag{1a}$$

where m is the mass of the muscle, c_p is the specific heat capacity, $\dot{T} = (dT/dt) =$ change in the temperature for the muscle, P is the power supplied to the muscle, T_∞ is the ambient temperature, $T - T_\infty = T_a$ (assume), h is the convective heat transfer coefficient, and A_c is the area of the coil. The thickness of the silver coating is very small (in nanometer) compared with the diameter of the polymer thread, and it can be ignored for simplicity. The lumped capacitance model captures the temperature profile very well as shown in Ref. [23], and it was used as a baseline to compare. Taking Laplace on both sides of Eq. (1*a*)

$$\frac{T_a}{P}(s) = \frac{\frac{1}{mc_p}}{s + \frac{hA_c}{mc_p}} = \frac{a}{s + b} \tag{1b}$$

rearranging and considering zero initial conditions.

From Eq. (1*a*), we can observe that the system should have a first-order transfer function with one pole and no zero, where s is a Laplace variable, $a = (1/mc_p)$ and $b = (hA_c/mc_p)$. However, this model is based on lumped parameter assumption and ignores other heat transfer modes such as radiation and non-constant convective heat transfer coefficient, which make it a higher-order and nonlinear system. Therefore, exploring higher-order TFs also makes sense to predict the output of the muscle closely. In the lumped capacitance model, if the actuator is represented as two connected systems each with first-order thermal system, then two first-order system transfer function may result in a second-order system. This aspect should be investigated further.

Similarly, for the thermomechanical system, the change in energy of the system would cause linear stroke and the twisting moment when subjected to an external load. However, the twisting moment is insignificant when compared to the external load. Table 1 summarizes all the combination of transfer functions with their fitting for the system up to third order. We compared the first, second, and third orders of the transfer function (shown as TF_{TP}, $TF_{TP2,}$ and $TF_{TP3,}$ respectively, in Fig. 5) for both electrothermal (Fig. 5(i)) and thermomechanical models (Fig. 5(ii)).

The second-order electrothermal transfer function (TF_1) was chosen for further study. This TF has 90% accuracy (mean square error (MSE) of 8.389) and is given as

$$TF_1 = \frac{-2.072\,s + 6.622}{s^2 + 2.112\,s + 0.1259} = \frac{T(s)}{P(s)} \tag{2a}$$

The thermomechanical transfer function chosen was a first-order system with 93% accuracy (MSE, 0.001362), and transfer function (TF_2) is provided in the following equation:

$$TF_2 = \frac{0.02032\ \ s + 0.003318}{s + 0.2947} = \frac{F\ (s)}{T\ (s)} \tag{2b}$$

The two transfer functions were used in series to predict the electro-thermo-mechanical behavior of the system. The block diagram of the Simulink model used to compare and evaluate the TFs is shown in Fig. 5(iii). Further, the MSE presented in this paper was calculated using the MATLAB®. The model (force: power) was validated using the available data, as shown in Fig. 6. The MSE between the simulated and experimental results was found to be 0.145, 0.239, and 0.295, respectively, for the 2.5-A, 2.7-A, and 2.9-A current inputs (34 W, 40 W, and 47 W power inputs).

3.3 Dynamic Modeling: Euler–Lagrangian Modeling. The schematic diagram of the robotic finger is shown in Fig. 7 consisting of three phalanges, which correspond to the proximal, middle, and distal phalanges. We have used the Euler–Lagrangian approach for the dynamic modeling of the index finger to determine the velocity Jacobians. The offset "e" for the tendon is assumed to be a constant value of 4.5 mm. The modeling approach follows the one described by Spong et al. [24].

The following assumptions are made for the modeling of the finger dynamics: (1) the friction between the links is negligible, (2) tendon movement is smooth and experiences no jerk while passing through guides, (3) all the springs have the same properties, and (4) the input force and temperature profiles of the actuator (TCP

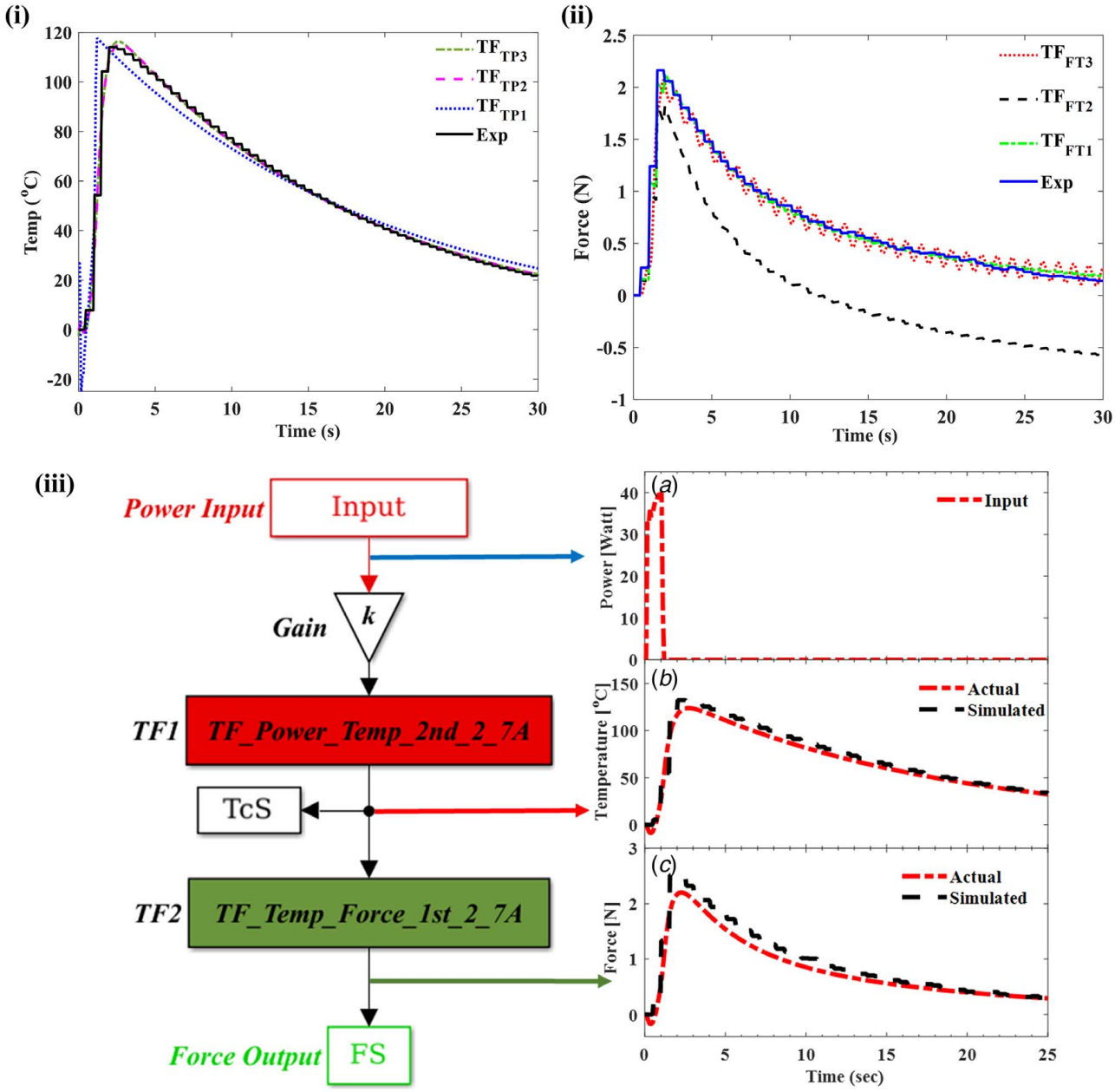

Fig. 5 Comparison of different order transfer functions for (i) electrothermal system using power as an input and temperature as an output, (ii) thermomechanical system using temperature as an input and force as an output, and (iii) block diagram of the Simulink® model used for predicting the output behavior of the TCP muscle used in the hand where power is the input and force is the output. This model will be used for comparing PIS, FIS, and experimentally measured angles.

muscle) are known prior from the experimental results. The general equation for the Euler–Lagrangian modeling is as follows:

$$\frac{d}{dt}\left(\frac{\partial K}{\partial \dot{q}_i}\right) - \left(\frac{\partial K}{\partial q_i}\right) + \frac{\partial P}{\partial q_i} = \tau_i \tag{3}$$

where K, P, and τ_i are kinetic energy, potential energy, and torque of the ith joint, respectively.

In the special case of a three-link robotic manipulator [24], (Eq. (3)) can be written as

$$\sum_j d_{kj}\ddot{q}_j + \sum_{i,j}\left\{\frac{\partial d_{kj}}{\partial q_i} - \frac{1}{2}\frac{\partial d_{ij}}{\partial q_k}\right\}\dot{q}_i\dot{q}_j + \frac{\partial P}{\partial q_k} = \tau_k \tag{4}$$

This equation is expanded for three links and yields the following equation set:

$$\begin{aligned}\tau_1 = {} & d_{11}\ddot{q}_1 + d_{12}\ddot{q}_2 + d_{13}\ddot{q}_3 + C_{111}\dot{q}_1^2 + C_{221}\dot{q}_2^2 + C_{331}\dot{q}_3^2 \\ & + (C_{211} + C_{121})\dot{q}_1\dot{q}_2 + (C_{311} + C_{131})\dot{q}_3\dot{q}_1 \\ & + (C_{321} + C_{231})\dot{q}_2\dot{q}_3 + \phi_1 + \tau_{d1}\end{aligned} \tag{5a}$$

$$\begin{aligned}\tau_2 = {} & d_{21}\ddot{q}_1 + d_{22}\ddot{q}_2 + d_{23}\ddot{q}_3 + C_{112}\dot{q}_1^2 + C_{222}\dot{q}_2^2 + C_{332}\dot{q}_3^2 \\ & + (C_{212} + C_{122})\dot{q}_1\dot{q}_2 + (C_{312} + C_{132})\dot{q}_3\dot{q}_1 \\ & + (C_{322} + C_{232})\dot{q}_2\dot{q}_3 + \phi_2 + \tau_{d2}\end{aligned} \tag{5b}$$

$$\begin{aligned}\tau_3 = {} & d_{31}\ddot{q}_1 + d_{32}\ddot{q}_2 + d_{33}\ddot{q}_3 + C_{113}\dot{q}_1^2 + C_{223}\dot{q}_2^2 + C_{333}\dot{q}_3^2 \\ & + (C_{213} + C_{123})\dot{q}_1\dot{q}_2 + (C_{313} + C_{133})\dot{q}_3\dot{q}_1 \\ & + (C_{323} + C_{233})\dot{q}_2\dot{q}_3 + \phi_3 + \tau_{d3}\end{aligned} \tag{5c}$$

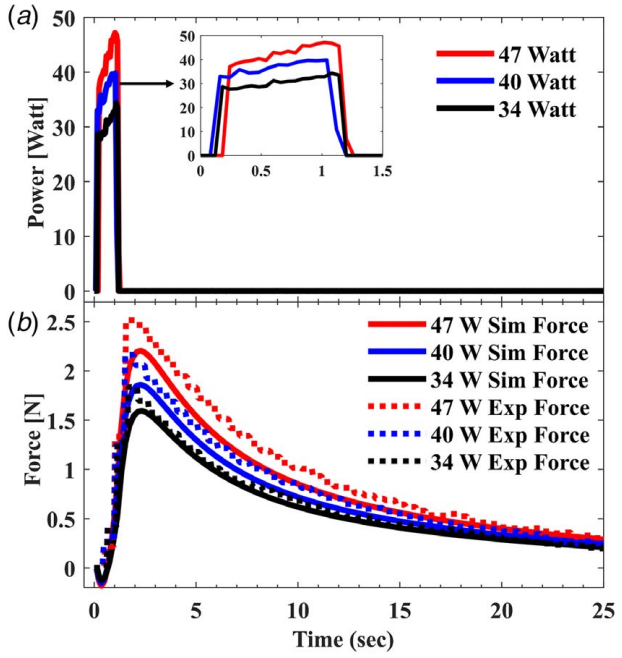

Fig. 6 (*a*) Experimental input power provided to the muscle and (*b*) experimental and predicted force using the coupled model (TF_1 and TF_2)

where τ_k is the torques experienced by the link k, d_{kj} is the inertia matrix, $\ddot{q}$ is the angular acceleration, $\dot{q}$ is the angular velocity, q is the angular displacement, C_{ijk} is the Coriolis components of acceleration, and ϕ_k is the potential energy derivatives consisting of gravity and passive spring (K) terms.

The full derivation of the Eq. (5) and the Simulink® model used for numerical simulations are documented in a supporting file [26]. We have ignored the terms in the model, which do not have significant effects (very small in order, $\sim 10^{-10}$) such as Coriolis terms and all the terms of inertia matrix except the diagonal terms. But in the Eq. (5), we have added one extra damping term, i.e., $\tau_{di} = c_d\ \dot{q}_i$ ($i = 1, 2, 3$), which is proportional to the angular velocity of the link $\dot{q}_i$. A similar modification of dynamic the equation was presented by Lewis et al. [27]. Damping exists in human fingers as well as in robotic finger joints, which helps control (reduces oscillations).

Assuming the torque generated by the TCP actuator is distributed at each joint (τ_1 = MCP joint, τ_2 = PIP joint, and τ_3 = DIP joint;) with certain factors, the torques can be written as

$$\tau_3 = \gamma\tau, \quad \tau_2 = \beta\tau, \quad \tau_1 = \alpha\tau, \quad \tau = Fe \tag{6}$$

where F is the force generated by the TCP actuator and e is the offset distance of the tendon. α, β, and γ are the fractions of torque on each joint. These parameters can be determined based on the design and configuration of the finger. Zollo et al. [28] and Carrozza et al. [29] have used similar assumptions to determine the applied torque at each joint. The values of α, β, and γ were initially obtained by comparing the simulated values (assuming $\alpha = \beta = \gamma = 1$) with the experimentally measured angles and varying them until all the three simulated angles matched the experimental values. The final values were found to be 0.25, 0.22, and 0.20, respectively, which were kept constant and used for the rest of the study. Also, the friction in the force transmission is almost negligible for such system as described in one of our previous study, which is found to be around 0.14 N when compared to the 3 N produced by TCP muscle.

4 Simulation of Finger Motions

Two types of simulations were performed, the first one is done using the experimentally measured force of the TCP muscle as the input (obtained from the load cell). We will refer to it as *force input-based simulation* (FIS) in the text. These force data were multiplied by the offset value e to determine the torque experienced by the finger (Fig. 8(*a*), left). These torque values were supplied to the Simulink® model to obtain the finger joint variables (angles and angular velocities) using Eqs. (5)–(6). The second type of simulation is performed using the two transfer functions in series for electrothermal and thermomechanical model obtained from the system identification as discussed in Section 3.2. We provided the experimentally measured power as an input and obtained the force, which was multiplied by an offset distance to obtain torque. We will refer this as *power input-based simulations* (PIS) in the text. Further, the simulations from these models (FIS and PIS) were compared with the experimentally measured angles as described in Section 5.

The simulations were performed using the Simulink® (MATLAB® R2017a) model by directly implementing the analytical equations of motion (torque of a three-link) coupled with the transfer functions.

Several simulations were performed by varying the damping factor c_d until the experimentally measured angles, under the same conditions, were bounded closely by the simulation results. The damping factor is comparable with the one used by others [30] for such simulations. It was kept constant after finding the

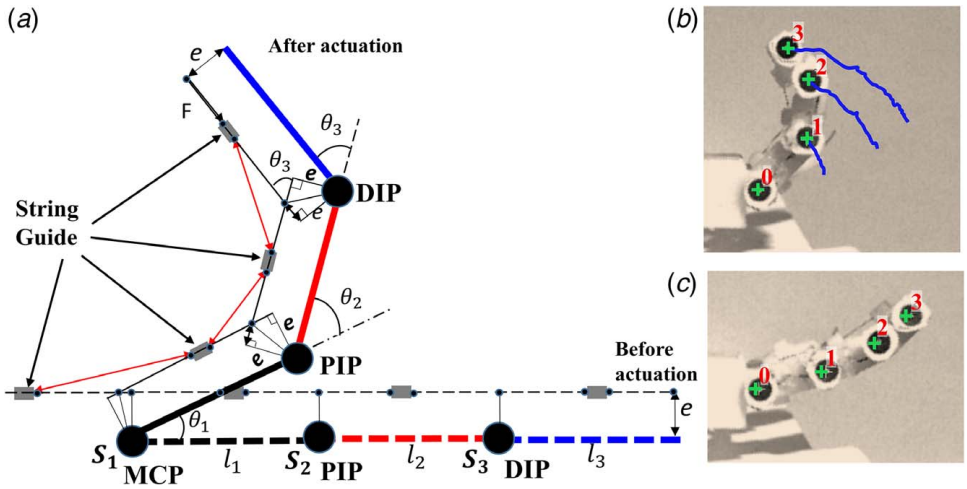

Fig. 7 (*a*) Free body diagram of the finger, (*b*) the prototype hand after actuation, and (*c*) prototype hand before actuation

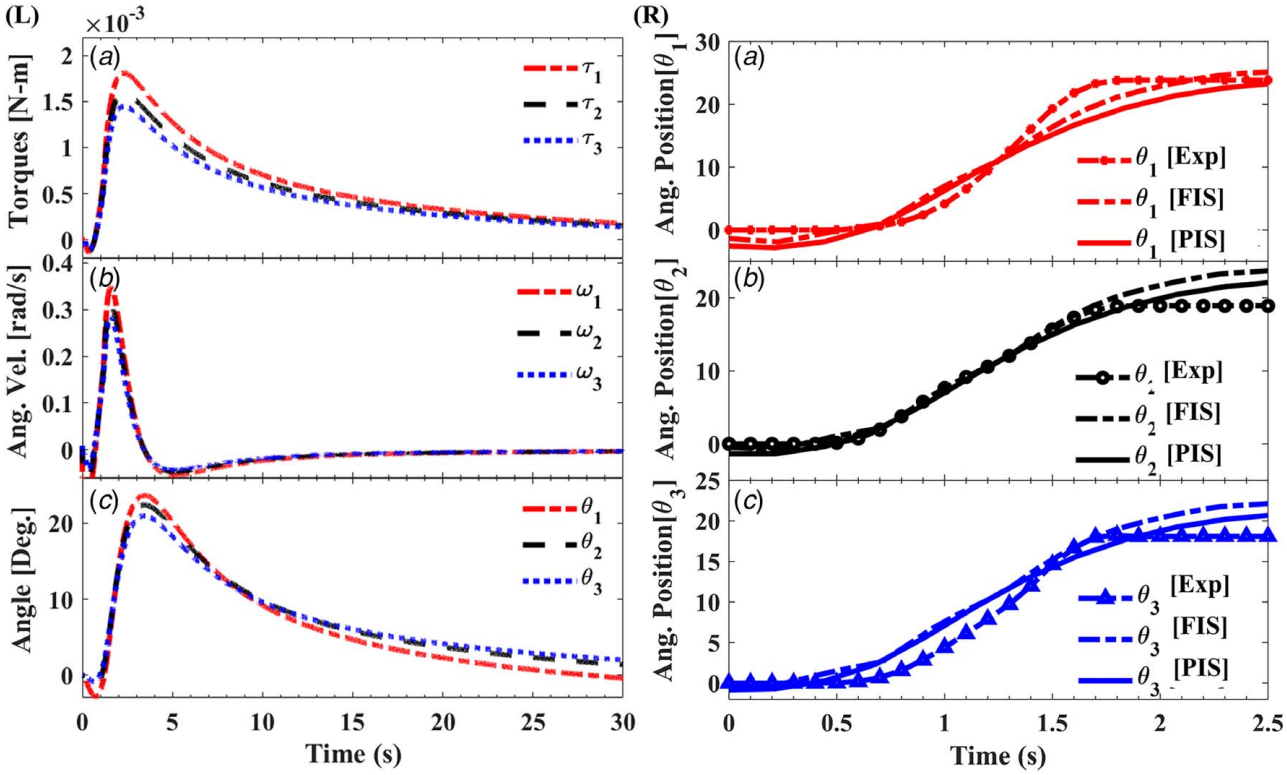

Fig. 8 (L) shows force as an input (FIS) simulation results at 2.5 A current (3.4 W/cm) and (R) comparative representation of experimentally measured values, FIS, and PIS for validation of the model. θ_i [Exp], θ_i [FIS], and θ_i [PIS] represent the results obtained from experimental measurements, FIS and PIS ($i = 1, 2, 3$), respectively.

Table 2 Simulation parameters

Parameter	Value
Mass of link 1 (m_1)	5.85×10^{-4} kg
Mass of link 2 (m_2)	4.50×10^{-4} kg
Mass of link 3 (m_3)	3.91×10^{-4} kg
Moment of inertia (i_1)	6.26×10^{-6} kg m^2
Moment of inertia (i_2)	5.55×10^{-6} kg m^2
Moment of inertia (i_3)	6.76×10^{-6} kg m^2
Simulation time	45 s (regular actuation)
Input force	3 N
Offset distance (e)	4.5×10^{-3} m
Length of link 1 (l_1)	1.2×10^{-2} m
Length of link 2 (l_2)	9.0×10^{-3} m
Length of link 3 (l_3)	1.2×10^{-2} m
Damping factor (C_d)	1×10^{-3} N ms/rad
Spring constant (theoretical)[a]	5.23×10^{-4} N m/deg
Spring constant (exp. mean) (K)	6.12×10^{-4} N m/deg

[a]The spring constants were determined based on the equation for a torsional spring, considering the wire diameter, number of windings, and modulus of rigidity.

value initially by trials. All the simulation parameters are presented in Table 2, and the simulation results will be discussed in Section 5.

5 Results and Discussions

Three amplitudes of the power (34 W, 40 W, and 47 W) were provided to the three-ply muscle (100 mm long) integrated into the hand. The power per unit length of the muscle is often used to describe the electrical power needed for the TCP muscles. We describe the power given to the muscles as the absolute power (W) as well as the power per loaded length (W/cm) alternatively in this manuscript while discussing about power consumption. We used the measured FIS and PIS for the simulation, and the simulations were compared with the experimental results.

5.1 Simulation, Analysis, and Comparison at Three Different Power Values. Here, experiments were performed for the finger flexion at three different power values of 3.4 W/cm, 4.0 W/cm, and 4.7 W/cm (corresponding current 2.5 A, 2.7 A, and 2.9 A, respectively) for a duration of 1 s. As a summary of this comparative analysis, the key values from Figs. 8–10 are presented in the Table 3. These values include maximum angular displacement obtained from experiments and the simulations of the three joints of the finger during flexion motion. The plots in the left side of Figs. 8–10 show the results from FIS. In other words, the torques in the subplots (*a*) were obtained by multiplying the offset with the forces as described earlier for FIS. The subplots (*b*) illustrate the velocity profiles of the finger joints and the subplot (*c*) show the corresponding angles of all three joints of the finger. Further, the simulated angles given as $\theta_{1,2,3}$ [FIS] and $\theta_{1,2,3}$ [PIS] were compared with the experimental results as shown in the right side of the Figs. 8–10. The experimental values of the joint angles were obtained by tracking joint angles from the video at 30 fps and PCC® (Phantom Camera Control) software.

The plots on the right side of Figs. 8–10 validate our model by depicting the closeness of simulated values with the experimental values. We can observe that the curves representing angular displacements follow a similar path with a small mean square error. At all these three power values, the highest error is for the PIP joint (Fig. 9) due to the underactuated nature of the mechanism. These results confirm the validity of this model to predict the flexion motion of the finger actuated using TCP muscles. Further, we observe that the increase in error with the increase in the input power, which is partially due to the change in the heat

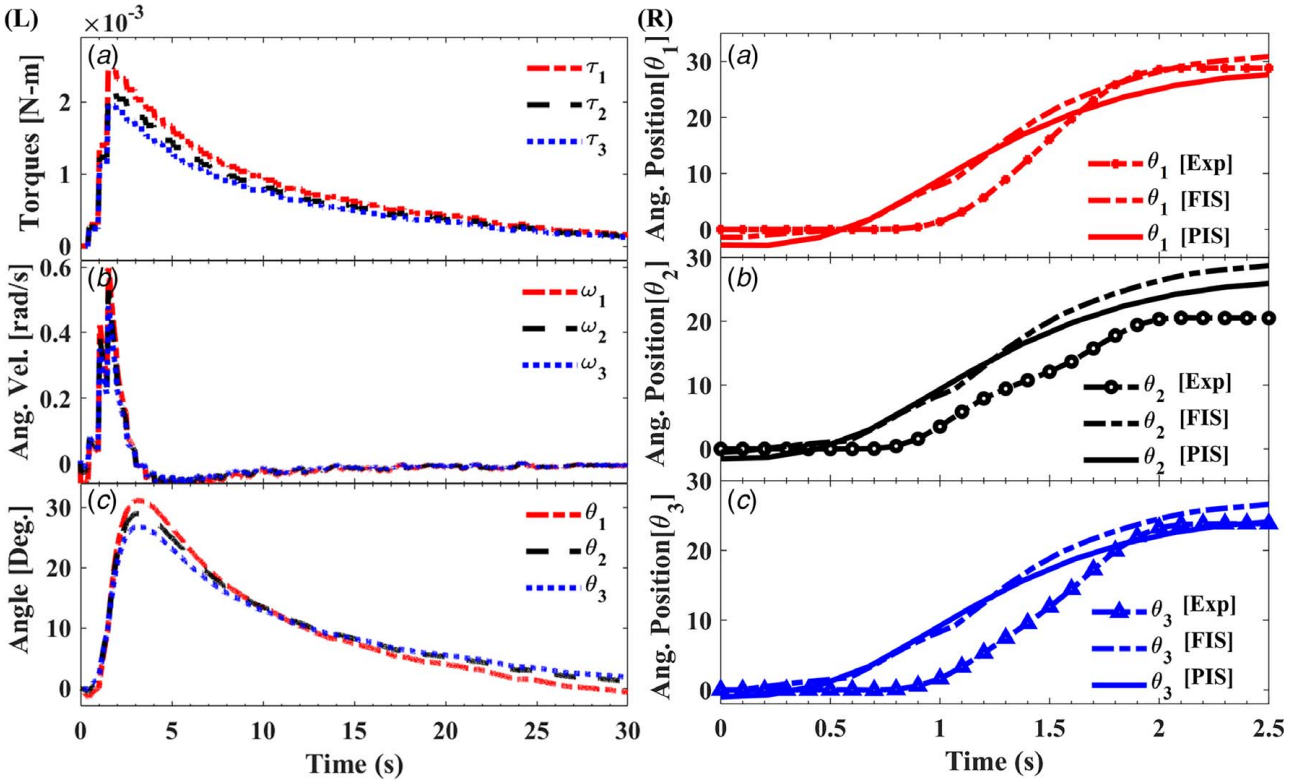

Fig. 9 (L) shows FIS results at 2.7 A current (4.0 W/cm) and (R) comparative representation of experimentally measured values, FIS, and PIS for validation of the model. θ_i [Exp], θ_i [FIS], and θ_i [PIS] are given as displayed in Fig. 8.

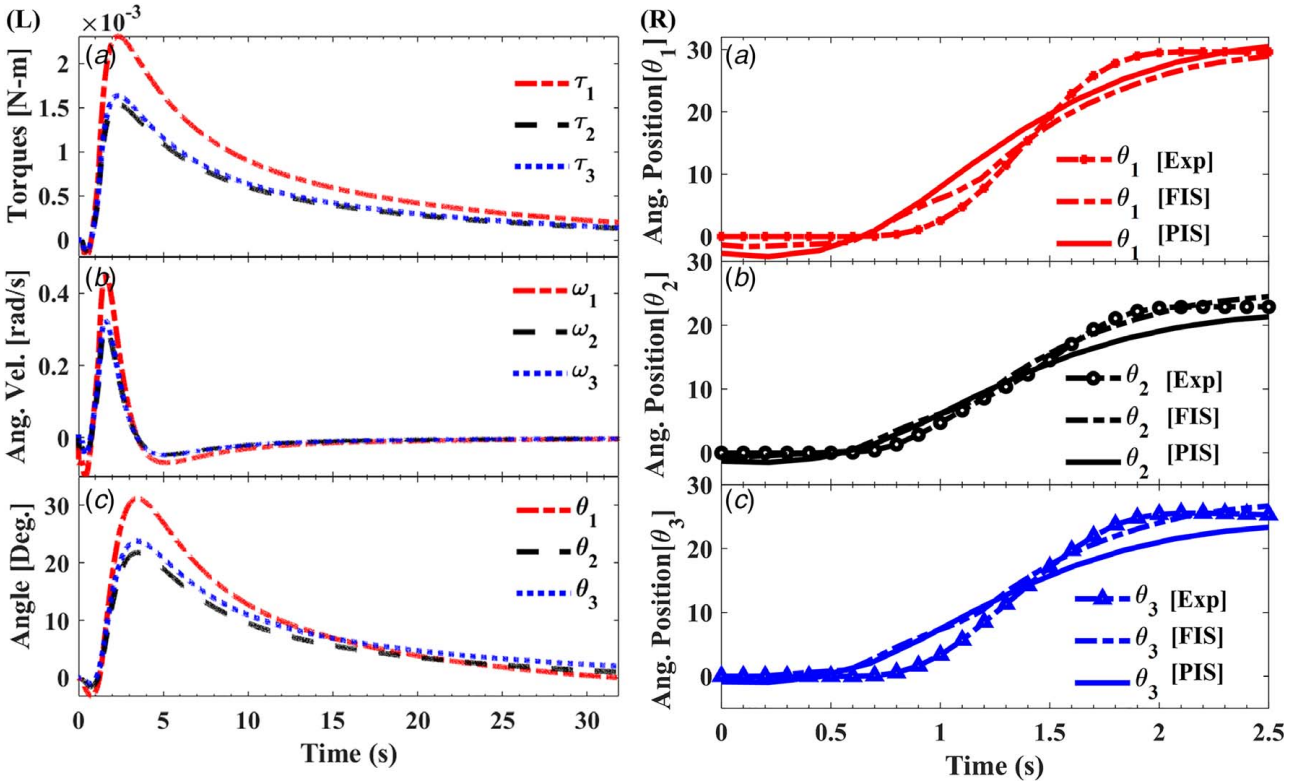

Fig. 10 (L) shows FIS results at 2.9 A current (4.7 W/cm) and (R) is the comparative representation of experimentally measured values, FIS, and PIS for validation of the model. θ_i [Exp], θ_i [FIS], and θ_i [PIS] are given as displayed in Fig. 8.

Table 3 Summary of the results obtained from experimental and simulation

	MCP (θ_1)	PIP (θ_2)	DIP (θ_3)	Power
Max angle [Exp]	24 deg	19 deg	18 deg	3.4 W/cm @ 2.5 A for 2.0 s
[FIS]	25.5 deg	24 deg	22.4 deg	
[PIS]	23.7 deg	22.5 deg	21 deg	
Max angle [Exp]	28.8 deg	20.5 deg	23.8 deg	4.0 W/cm @ 2.7 A for 2.0 s
[FIS]	31 deg	29 deg	26.8 deg	
[PIS]	28 deg	26.3 deg	24.4 deg	
Max angle [Exp]	29.6 deg	22.9 deg	25.6 deg	4.7 W/cm @ 2.9 A for 2.0 s
[FIS]	29.6 deg	25 deg	27 deg	
[PIS]	31 deg	21.8 deg	23.7 deg	

dissipation rate and the effect of the friction resulting from limited intercoil spacing of the muscle at elevated temperature (nonlinearity increases at the elevated temperature for such polymer actuators).

Interestingly, the flexion finger velocity reaches up to 34.37 deg/s for the flexion motion. However, friction and nonlinearity (such as the coil's contact in the TCP [2]) may play a critical role which can be observed again from the increasing error with the increase in velocity except for the MCP at 4.7 W/cm (Fig. 10). Also, with the increase in power and consequently an increase in the muscle temperature, lesser dominant modes of heat transfer such as radiation and variable convective heat transfer start to play a key role along with friction and nonlinearity. Moreover, refereeing the figures, the error between FIS and PIS results looks very similar, which suggests that most of the error comes from the finger model (consistent with the sensitivity analysis). Note that we did not present the torque, angular velocity, and angle plots for PIS simulation (like the three subplots in the left of Figs. 8–10), but we only provided the final simulation results (θ_i [PIS]) to limit the figure numbers and the scope of the study.

Therefore, the study suggested that friction and nonlinearity should not be ignored to make a better model under certain input conditions. The PIS can be used to predict the joint angles because the intermediate variables (force and temperature) would be calculated based on the input power value.

5.2 Sensitivity Analysis. A sensitivity analysis of the dynamic Eq. (5) for a variation in the mass (Mass), inertia (Inertia) damping factor (Damp), and spring constant (K) of the robotic finger was performed. Power as input simulation was used to perform this study. The results presented in Fig. 11(i) show that mean square error values for doubling the mass are 10.67 deg, 1.46 deg, and 0.13 deg for MCP, PIP, and DIP, respectively. If the mass of each link is reduced by half, the MSE changes to 2.60 deg, 0.35 deg, and 0.03 deg for the MCP, PIP, and DIP respectively. Further, the sensitivity analysis for the inertia (Fig. 11(ii)) shows little or no effect whereas doubling the inertia causes MSE 0.0122 deg, 0.0094 deg, and 0.0068 deg and making inertia half would make MSE 0.0020 deg, 0.0015 deg, and 0.001 deg for MCP, PIP, and DIP joints, respectively.

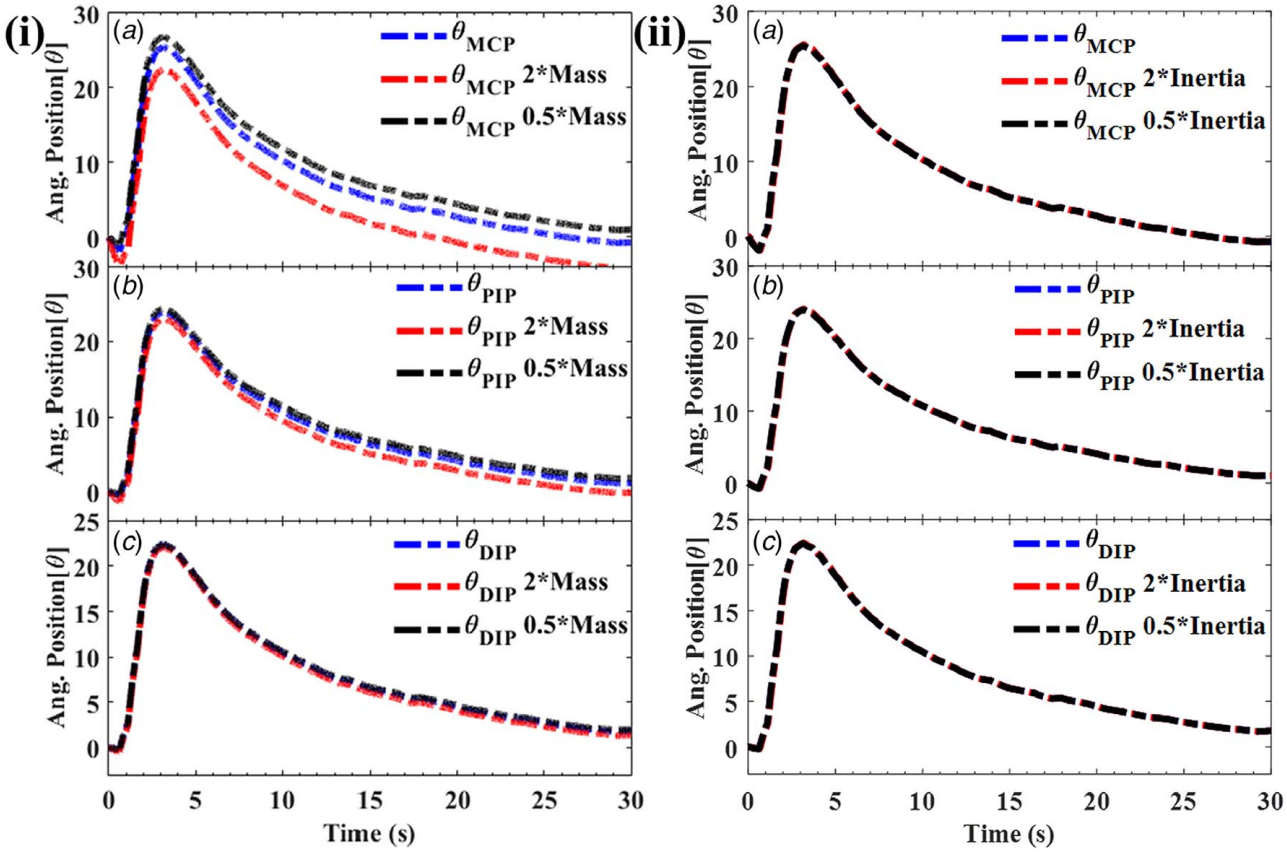

Fig. 11 Sensitivity analysis on the simulation results (i) for mass variation and (ii) for inertia variation

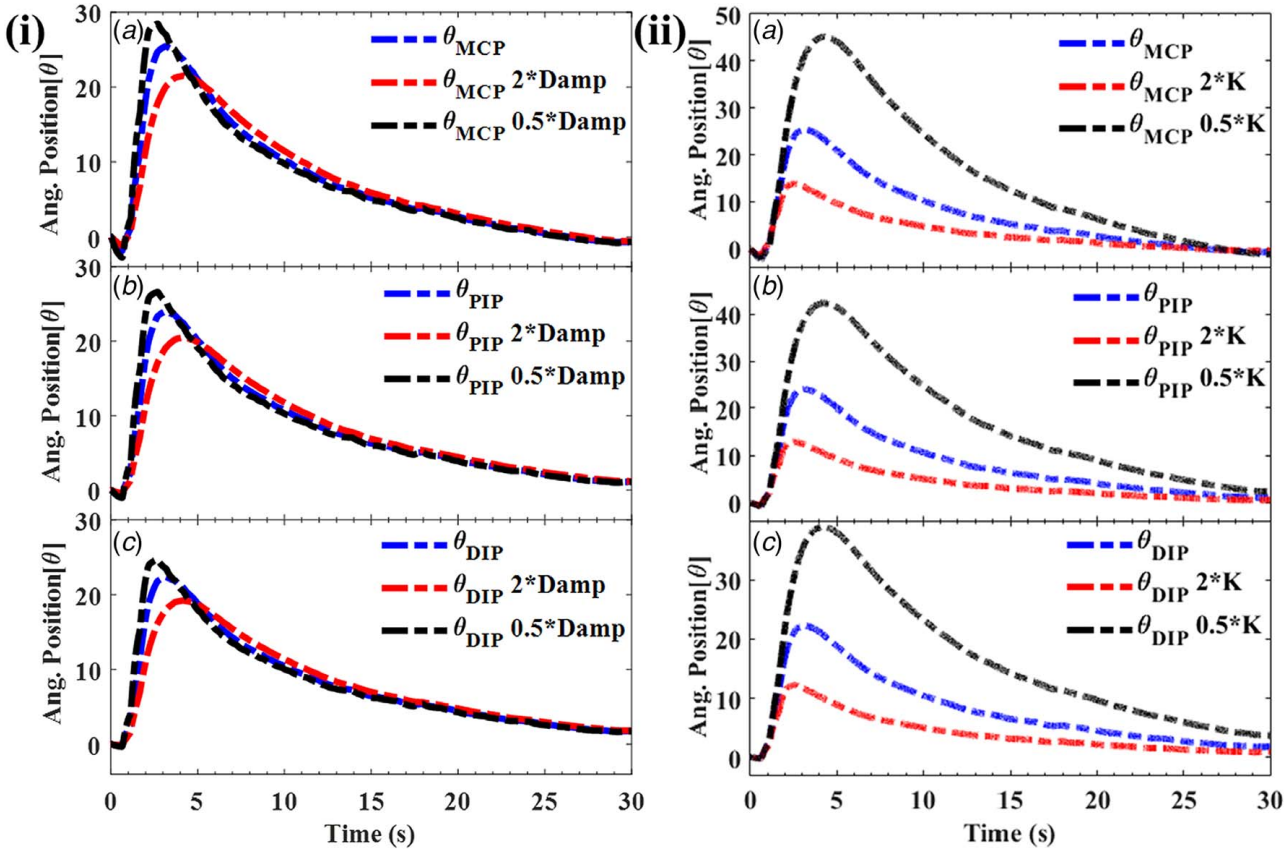

Fig. 12 Sensitivity analysis on the simulation results (i) for damping factor variation and (ii) for spring constant (*K*)

Variation in the damping factors also affects the output of the model. Doubling the damping factor would result in an MSE of 3.21 deg, 2.67 deg, and 2.21 deg whereas reducing the damping factor by half would make MSE 1.63 deg, 1.30 deg, and 1.04 deg respectively, as shown in Fig. 12(i).

The model is very sensitive to the spring constant (K) values as shown in Fig. 12(ii). If we change the spring constant by double, the resulting MSE for the MCP, PIP, and DIP joints would be 26.60 deg, 26.15 deg, and 23.77 deg, respectively, whereas if we half the value of K, the respective MSE values would be 113.62 deg, 107.90 deg, and 92.17 deg. The significant change in MSE for different joints illustrates that the spring constant plays a vital role in the finger flexion motion. If the spring constant is much higher, then the flexion angle will be small, and vice versa.

Sensitivity analysis shows the impact of the change in physical parameters on the dynamics of the system and as expected spring constant can influence the motion drastically. This study is important in selecting the actuator configuration and parameters that result in certain actuation performance such as maximum angles and time-domain characteristics in response to input conditions.

6 Conclusion

This paper described an electro-thermo-mechanical model coupled with the Euler–Lagrangian (E–L) approach for modeling, simulation, and experimental validation of a robotic finger actuated by twisted and coiled polymer muscles. The TCP muscles are novel actuators that are presented in recent years, and there are no papers in the literature that show such a study about the coupled dynamic systems (the TCP muscle and the multi-joint robotic finger). The E–L method was employed for dynamic modeling of the finger, and system identification-based model was developed for the silver-coated TCP muscles. The two transfer functions were used in series to replicate the electro-thermo-mechanical behavior of the muscles/actuators. Further, a Simulink® model based on the derived equation set was developed to perform numerical simulations. Parameters were measured experimentally for TCP muscles for the coupled system. Particularly, the power input and the force profile (output in response to input electrical power) of the three-ply TCP muscle was used as an input to the Simulink® model. This study presents a method, which can be utilized for study of other under-actuated robotic hand models employing actuators such as SMA or TCP. Moreover, a sensitivity analysis of the model was performed for variation in link mass, inertia, damping factor, and spring constant. Future work would involve using the results of this dynamic modeling for the control and 3D dynamic equation for all the five fingers.

Funding data

- Office of Naval Research (ONR) (Grant No. N00014-15-1-2503; Funder ID: 10.13039/100000006).

References

[1] Belter, J. T., Segil, J. L., Dollar, A. M., and Weir, R. F., 2013, "Mechanical Design and Performance Specifications of Anthropomorphic Prosthetic Hands: A Review," J. Rehabil. Res. Dev., **50**(5), pp. 599–618.

[2] Haines, C. S., Lima, M. D., Li, N., Spinks, G. M., Foroughi, J., Madden, J. D., Kim, S. H., Fang, S., de Andrade, M. J., and Göktepe, F., 2014, "Artificial Muscles From Fishing Line and Sewing Thread," Science, **343**(6173), pp. 868–872.

[3] Wu, L., Jung de Andrade, M., Saharan, L., Rome, R., Baughman, R., and Tadesse, Y., 2017, "Compact and Low-Cost Humanoid Hand Powered by Nylon Artificial Muscles," Bioinspiration Biomimetics, **12**(2), p. 026004.

[4] She, Y., Li, C., Cleary, J., and Su, H.-J., 2015, "Design and Fabrication of a Soft Robotic Hand With Embedded Actuators and Sensors," ASME J. Mech. Rob., **7**(2), p. 021007.

[5] Tadesse, Y., Hong, D., and Priya, S., 2011, "Twelve Degree of Freedom Baby Humanoid Head Using Shape Memory Alloy Actuators," ASME J. Mech. Rob., **3**(1), p. 011008.

[6] Saharan, L., de Andrade, M. J., Saleem, W., Baughman, R. H., and Tadesse, Y., 2017, "iGrab: Hand Orthosis Powered by Twisted and Coiled Polymer Muscles," Smart Mater. Struct., **26**(10), p. 105048.

[7] Arjun, A., Saharan, L., and Tadesse, Y., 2016, "Design of a 3D Printed Hand Prosthesis Actuated by Nylon 6-6 Polymer Based Artificial Muscles," 2016 IEEE International Conference on Automation Science and Engineering (CASE), Fort Worth, TX, Aug. 21, pp. 910–915.
[8] Wu, L., Jung de Andrade, M., Rome, R. S., Haines, C., Lima, M. D., Baughman, R. H., and Tadesse, Y., "Nylon-Muscle-Actuated Robotic Finger," Proceedings of SPIE, 2015 Smart Structures and Materials, San Diego, CA.
[9] Saharan, L., and Tadesse, Y., 2016, "A Novel Design of Thermostat Based on Fishing Line Muscles," Proceedings of the ASME 2016 International Mechanical Engineering Congress and Exposition, Phoenix, AZ, Nov. 11–17, American Society of Mechanical Engineers, New York, p. V014T007A019.
[10] Saharan, L., and Tadesse, Y., 2019, "Novel Twisted and Coiled Polymer Artificial Muscles for Biomedical and Robotics Applications," *Materials for Biomedical Engineering*, A.-M. Holban and M. Grumezescu, eds., Elsevier, pp. 45–75l.
[11] Saharan, L., and Tadesse, Y., 2016, "Robotic Hand With Locking Mechanism Using TCP Muscles for Applications in Prosthetic Hand and Humanoids," Proceedings of Bioinspiration, Biomimetics, and Bioreplication 2016, International Society for Optics and Photonics, Las Vegas, NV, Aug. 12, p. 97970V.
[12] Tadesse, Y., Wu, L., and Saharan, L. K., 2016, "Musculoskeletal System for Bio-Inspired Robotic Systems," Mech. Eng. Mag., **138**(3), pp. S11–S16.
[13] Sharma, A., Saharan, L., and Tadesse, Y., 2017, "3-D Printed Orthotic Hand With Wrist Mechanism Using Twisted and Coiled Polymeric Muscles," Proceedings of ASME 2017 International Mechanical Engineering Congress and Exposition, Tampa, FL, Nov. 3–9, American Society of Mechanical Engineers, New York, p. V003T04A057.
[14] Cherubini, A., Moretti, G., Vertechy, R., and Fontana, M., 2015, "Experimental Characterization of Thermally-Activated Artificial Muscles Based on Coiled Nylon Fishing Lines," AIP Adv., **5**(6), p. 067158.
[15] Cho, K. H., Jung, H. S., Yang, S. Y., Kim, Y., Rodrigue, H., Moon, H., Koo, J. C., and Choi, H. R., 2019, "Sliding Filament Joint Mechanism: Biomimetic Artificial Joint Mechanism for Artificial Skeletal Muscles," ASME J. Mech. Rob., **11**(2), p. 021004.
[16] Mirvakili, S. M., Ravandi, A. R., Hunter, I. W., Haines, C. S., Li, N., Foroughi, J., Naficy, S., Spinks, G. M., Baughman, R. H., and Madden, J. D., 2014, "Simple and Strong: Twisted Silver Painted Nylon Artificial Muscle Actuated by Joule Heating," Proceedings of SPIE Smart Structures and Materials, San Diego, CA, Mar. 26, p. 90560I.
[17] Edmonds, B. P., and Trejos, A. L., 2017, "Stiffness Control of a Nylon Twisted Coiled Actuator for Use in Mechatronic Rehabilitation Devices," Proceedings of 2017 International Conference on Rehabilitation Robotics (ICORR), London, July 17–20, IEEE, New York, pp. 1419–1424.
[18] Schimmack, M., Feistauer, E. E., Amancio-Filho, S. T., and Mercorelli, P., 2017, "Hysteresis Analysis and Control of a Metal-Polymer Hybrid Soft Actuator," Energies, **10**(4), p. 508.
[19] Abbas, A., and Zhao, J., 2017, "A Physics Based Model for Twisted and Coiled Actuator," Proceedings of 2017 IEEE International Conference on Robotics and Automation (ICRA), Singapore, May 29–June 3, IEEE, New York, pp. 6121–6126.
[20] Yip, M. C., and Niemeyer, G., 2017, "On the Control and Properties of Super-coiled Polymer Artificial Muscles," IEEE Trans. Rob., **33**(3), pp. 689–699.
[21] Jafarzadeh, M., Wu, L., and Tadesse, Y., 2017, "System Identification of Force of a Silver Coated Twisted and Coiled Polymer Muscle," Proceedings of the International Mechanical Engineering Congress and Exposition (IMECE 2017), Tampa, FL, Nov. 3–9, p. V04BT05A027.
[22] Arakawa, T., Takagi, K., Tahara, K., and Asaka, K., 2016, "Position Control of Fishing Line Artificial Muscles (Coiled Polymer Actuators) From Nylon Thread," Proceedings of SPIE Smart Structures and Materials, International Society for Optics and Photonics, Las Vegas, NV, Apr. 15, p. 97982W.
[23] Karami, F., and Tadesse, Y., 2017, "Modeling of Twisted and Coiled Polymer (TCP) Muscle Based on Phenomenological Approach," Smart Mater. Struct., **26**(12), p. 125010.
[24] Spong, M. W., Hutchinson, S., and Vidyasagar, M., 2006, *Robot Modeling and Control*, Wiley, New York.
[25] Saharan, L., and Tadesse, Y., 2016, "Fabrication Parameters and Performance Relationship of Twisted and Coiled Polymer Muscles," Proceedings of ASME 2016 International Mechanical Engineering Congress and Exposition, Phoenix, AZ, Nov. 11, American Society of Mechanical Engineers, New York, p. V014T11A028.
[26] Saharan, L., Wu, L., and Tadesse, Y., 2019, "Modeling and Simulation of Robotic Finger Powered by Nylon Artificial Muscles-Equations with Simulink Model," e-print arXiv:1901.09486.
[27] Lewis, F. L., Dawson, D. M., and Abdallah, C. T., 2003, *Robot Manipulator Control: Theory and Practice*, Taylor & Francis, London.
[28] Zollo, L., Roccella, S., Guglielmelli, E., Carrozza, M. C., and Dario, P., 2007, "Biomechatronic Design and Control of an Anthropomorphic Artificial Hand for Prosthetic and Robotic Applications," IEEE/ASME Trans. Mechatron., **12**(4), pp. 418–429.
[29] Carrozza, M. C., Suppo, C., Sebastiani, F., Massa, B., Vecchi, F., Lazzarini, R., Cutkosky, M. R., and Dario, P., 2004, "The SPRING Hand: Development of a Self-Adaptive Prosthesis for Restoring Natural Grasping," Auton. Rob., **16**(2), pp. 125–141.
[30] Ozawa, R., Bae, J.-H., and Arimoto, S., 2006, "Multi-Fingered Dynamic Blind Grasping With Tactile Feedback in a Horizontal Plane," Proceedings 2006 IEEE International Conference on Robotics and Automation, 2006. ICRA 2006, Orlando, FL, May 15–19, IEEE, New York, pp. 1006–1011.